Geophysical Research Letters

RESEARCH LETTER
10.1029/2022GL099635

Satellite-Observed Vegetation Responses to Intraseasonal Precipitation Variability

Bethan L. Harris[1,2], Christopher M. Taylor[1,2], Graham P. Weedon[3], Joshua Talib[1], Wouter Dorigo[4], and Robin van der Schalie[5]

[1]UK Centre for Ecology & Hydrology, Wallingford, UK, [2]National Centre for Earth Observation, Wallingford, UK, [3]Met Office, Wallingford, UK, [4]Department of Geodesy and Geoinformation, TU Wien, Vienna, Austria, [5]Planet, Haarlem, The Netherlands

Key Points:

- Vegetation Optical Depth responds to intraseasonal precipitation variability in arid and semi-arid regions
- The phase difference of this response is usually less than 7 days, and is shortest for sparse vegetation
- After a wet intraseasonal period, the vegetation response can persist for over 2 months

Supporting Information:

Supporting Information may be found in the online version of this article.

Correspondence to:

B. L. Harris,
bethar@ceh.ac.uk

Citation:

Harris, B. L., Taylor, C. M., Weedon, G. P., Talib, J., Dorigo, W., & van der Schalie, R. (2022). Satellite-observed vegetation responses to intraseasonal precipitation variability. *Geophysical Research Letters*, *49*, e2022GL099635. https://doi.org/10.1029/2022GL099635

Received 19 MAY 2022
Accepted 11 JUL 2022

Abstract There is limited understanding of how vegetation responds to intraseasonal modes of rainfall variability despite their importance in many tropical regions. We use observations of precipitation and X-band Vegetation Optical Depth (VOD) from 2000 to 2018 to assess the relationships between rainfall and vegetation water content on 25–60-day timescales. Cross-spectral analysis identifies coherent intraseasonal relationships between precipitation and VOD, mostly in arid or semi-arid regions where vegetation is water-limited. Changes in VOD tend to lag anomalous rainfall, usually within 7 days. The fastest vegetation response is observed in sparsely vegetated areas (median 3 days). Following strong intraseasonal wet events, anomalously high VOD can persist for 2 months after the rainfall peak. This vegetation response can feed back onto the atmosphere, so improved representation of vegetation responses in models has the potential to improve subseasonal-to-seasonal forecasts.

Plain Language Summary It is difficult to predict temperature and rainfall more than 2 weeks in advance. Predictions at this timescale are helped by some common patterns of rainfall which cause wet and dry spells lasting from a few weeks to 2 months. Here, we use satellite measurements of rainfall and a vegetation metric that is strongly related to vegetation water content to study the relationships between these rainfall patterns and vegetation across the world. We find many regions where increased rainfall is followed by an increase in vegetation water content, usually with a delay of less than a week. This is most commonly seen in drier locations, where vegetation has a limited supply of water. After a wet spell, vegetation water content can persist above normal levels for over 2 months. This means that changes in vegetation caused by a wet or dry spell have the potential to affect rainfall in the next wet or dry spell, via changes in the energy and water transfers between the land and the atmosphere. Therefore, representing these vegetation responses correctly in models may lead to improvements in temperature and rainfall prediction weeks ahead.

1. Introduction

In recent years there has been substantial interest in improving the skill of subseasonal-to-seasonal (S2S; 2–8 weeks) forecasts, which sit between traditional weather and climate forecasts (Brunet et al., 2010; Vitart et al., 2017). A major source of global S2S predictability is provided by tropical intraseasonal oscillations (ISOs: Ding et al., 2011; Waliser et al., 2003), such as the Madden-Julian Oscillation (MJO), which produces rainfall fluctuations with a period of approximately 30–60 days (Madden & Julian, 1994). Accurate representation of the land surface and its interaction with the atmosphere is also key to developing skillful S2S forecasts. The state of the land surface (e.g., root zone soil moisture or leaf area) varies more slowly than the atmospheric state and affects the partitioning of the surface energy budget through changes in evapotranspiration, surface albedo and roughness. The land therefore provides a potential source of S2S predictability to the atmosphere (Dirmeyer et al., 2015, 2018; Guo et al., 2011). Realistic land surface initialization has been shown to enhance S2S predictability (Guo et al., 2011, 2012; Koster et al., 2010, 2020), and improved variability at S2S timescales may also provide skill (Zhu et al., 2019).

Intraseasonal land surface feedbacks impact circulation and rainfall in India (Ferranti et al., 1999; Saha et al., 2012; Unnikrishnan et al., 2017; Webster, 1983), South America (Chug & Dominguez, 2019; Spennemann & Saulo, 2015), Australia (Yu & Notaro, 2020) and West Africa (Lavender et al., 2010; Talib et al., 2022;

Taylor, 2008). For example, regional-scale soil drying and associated vegetation browning can induce an anomalous heat low which enhances rainfall via moisture convergence (Chug & Dominguez, 2019; Taylor, 2008).

Identifying where subseasonal precipitation variability drives surface flux dynamics has received little attention. One notable study showed strong responses of surface soil moisture (SSM) to the MJO with a lag of 2 days (Peng et al., 2017). Investigations of vegetation response to precipitation have mostly used monthly composites of Normalized Difference Vegetation Index (NDVI), with greenness typically lagging precipitation by 1–3 months (Nicholson et al., 1990; Papagiannopoulou et al., 2017; Seddon et al., 2016; Wu et al., 2015). However, these datasets cannot resolve response times shorter than 1 month. Regional investigations using 8- or 16-day NDVI composites have identified a 2–3-week lagged vegetation response (Justice et al., 1991; Cissé et al., 2016; J. Zhou et al., 2021).

NDVI needs to be composited over many days to obtain cloud-free images and minimize viewing angle effects. An alternative satellite vegetation metric, derived from passive microwave measurements and therefore generally unaffected by cloud cover, is Vegetation Optical Depth (VOD). VOD is a proxy for vegetation water content (Attema & Ulaby, 1978; Jackson & Schmugge, 1991; Meesters et al., 2005; van der Schalie et al., 2017) and also linked to aboveground biomass (Rodríguez-Fernández et al., 2018; Tian et al., 2016) and Gross Primary Productivity (GPP: Teubner et al., 2018; Wild et al., 2022). Recent studies have identified rapid L-band VOD responses to SSM variations: on average, vegetation water content peaks within 2 days of a soil moisture pulse across all observed land cover types (Feldman et al., 2018; Feldman, Short Gianotti et al., 2021; He et al., 2021).

Here we exploit daily VOD observations to produce the first global analysis quantifying vegetation responses to intraseasonal (25–60 day period) precipitation variability. Simulating vegetation dynamics at intraseasonal timescales is crucial for S2S models to benefit from land-based predictability. We use cross-spectral analysis to identify where, and at what lag, VOD responds to precipitation. We assess responses by land cover type and investigate VOD persistence following intraseasonal wet spells.

2. Data and Methods

2.1. Data

To investigate the vegetation response to intraseasonal precipitation variability, we use X-band (10.7 GHz) VOD observations from the Vegetation Optical Depth Climate Archive (VODCA) data set (Moesinger et al., 2020), which provides a long-term daily record (1997–2018) at 0.25° horizontal resolution. X-band provides good sensitivity to vegetation dynamics whilst also not becoming saturated too often. VODCA is constructed using the Land Parameter Retrieval Model (LPRM) v6 (van der Schalie et al., 2017), a forward radiative transfer model based on the model of Mo et al. (1982). LPRM is used to derive X-band VOD from the observations of four microwave radiometers (AMSR-E, AMSR2, TMI, WindSat). Observations over frozen ground or affected by radio-frequency interference are removed. Data from the different sensors are then averaged for each day after CDF-matching (Moesinger et al., 2020). We mask unphysical spikes in the VOD time series by comparing changes in consecutive observations with a monthly climatology for each pixel. We remove data points where both preceding and subsequent VOD changes exceed two standard deviations, as in Talib et al. (2022). This removes a mean of 1% of observed days from each pixel.

Inundation introduces artefacts into VOD data: increased surface water fraction produces an apparent decrease in VOD (Bousquet et al., 2021; Jones et al., 2011). This is due to the effect of open water on retrieved brightness temperatures, rather than a change in the vegetation itself. Previous studies have masked pixels containing more than 5% surface water (He et al., 2021; McColl et al., 2017; Tian et al., 2018). However, with such a mask, we still found widespread cases of day-to-day surface water fraction changes affecting VOD responses to rainfall. We therefore developed an alternative inundation mask, using daily SSM from the ESA CCI SM v06.1 combined active-passive microwave product (Dorigo et al., 2017; Gruber et al., 2019), and surface water fraction from the active-passive SWAMPS v3.2 data set (Jensen & Mcdonald, 2019), as in Talib et al. (2022), exploiting that artificial decreases in VOD due to inundation tend to coincide with increases in SSM. Further details are included in Text S1 in Supporting Information S1.

To analyze the relationships between VOD and precipitation, we use the Integrated Multi-satellitE Retrievals for GPM (IMERG) V06 product (Huffman et al., 2019), available from June 2000 onwards. We stratify data by

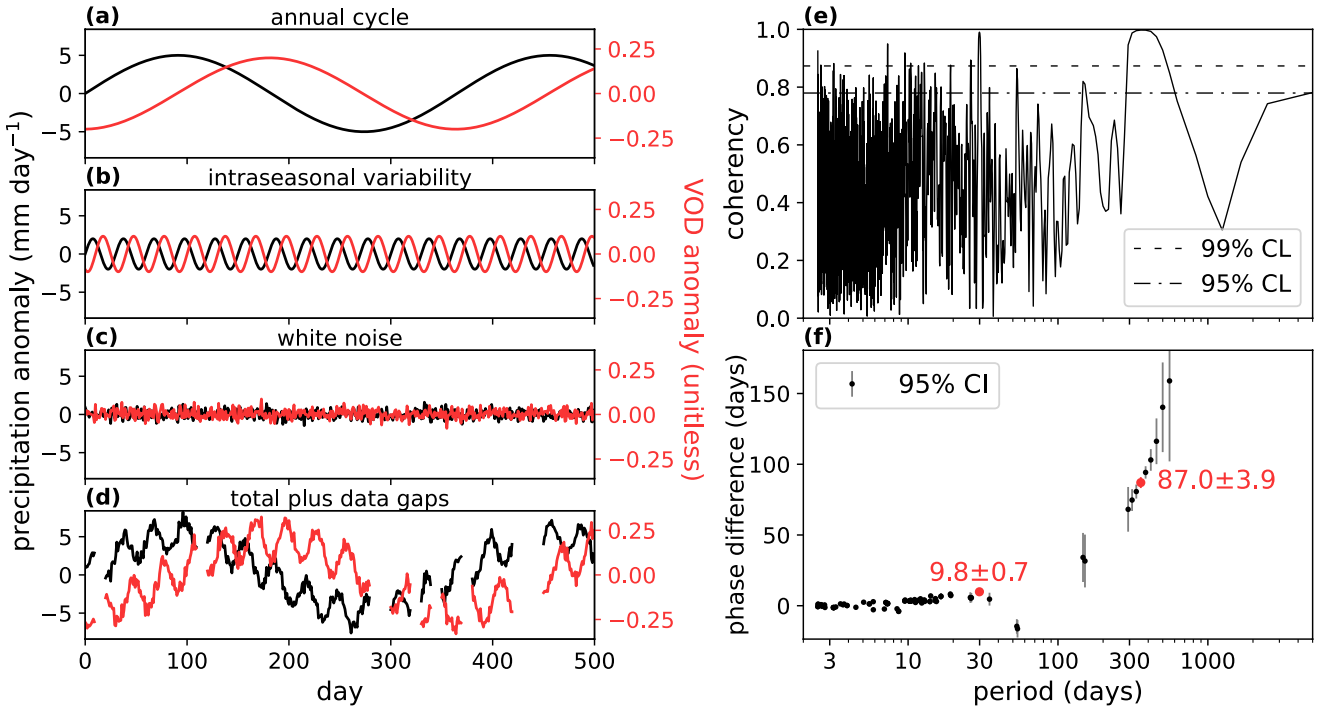

Figure 1. Illustration of cross-spectral analysis. Artificial annual cycles (a) and intraseasonal oscillations (b) of precipitation (black) and Vegetation Optical Depth (red) are added together, along with white noise (c), to create the total time series (d). Only the first 500 days of the 5,000-day time series are shown. Cross-spectral analysis computes the coherency (e) and phase difference (f) spectra. Dashed lines in (e) indicate the 95% and 99% confidence levels for coherency. Error bars in (f) show 95% confidence intervals for phase difference. Red markers and labels indicate the phase differences nearest the periods of the annual cycle and intraseasonal oscillation.

land cover type using the 2018 Copernicus Global Land Service Land Cover map (Buchhorn et al., 2020), and compare VOD behavior with NDVI using 16-day NDVI composites from 2000 to 2018 from the MODIS sensors onboard Aqua and Terra (Didan, 2015a, 2015b). All datasets are regridded to the 0.25° VOD grid.

2.2. Cross-Spectral Analysis

Cross-spectral analysis investigates the relationship between two variables as a function of frequency of variability. Here we analyze precipitation and VOD at intraseasonal (25–60-day) timescales across the tropics and mid-latitudes. Previous cross-spectral studies of precipitation and vegetation have been limited to specific regions and longer periods of variability (van Hoek et al., 2016; J. Zhou et al., 2021). Critically, we use Lomb-Scargle periodograms to derive cross spectra (coherency and phase spectra), allowing us to analyze time series with missing data (Weedon et al., 2015). This avoids the need for gap-filling, which would introduce bias to the spectra.

Figure 1 illustrates the principles of cross-spectral analysis for artificial precipitation and VOD time series. Both datasets comprise an annual cycle and an intraseasonal (30-day) oscillation, plus white noise (Figures 1a–1c). We mask 20% of the data in 10-day sections, to represent missing observations (Figure 1d). Coherency derived from Lomb-Scargle periodograms (Weedon et al., 2015) measures correlation between time series at a given frequency. Phase difference spectra describe the time by which one time series leads or lags the other. Phase differences are only plotted for periods at which the time series exhibit a coherent relationship significant at the 95% confidence level; for lower coherency, the error in the phase difference exceeds ±45°. A positive phase difference indicates that changes in VOD lag changes in precipitation. At each frequency, the phase difference is converted from degrees into days (i.e., [1/frequency] × phase difference[°]/360°).

As expected, Figure 1 demonstrates that coherency is high at periods of 30 and 365 days. The modeled annual cycle of VOD lags the annual cycle of precipitation by about 90 days (95% confidence interval 87.0 ± 3.9 days), while the intraseasonal variation in VOD lags the intraseasonal precipitation variation by 10 days (9.8 ± 0.7). The estimates of coherency and phase difference represent the average behavior. Therefore, the analysis may be biased in regions where the vegetation response to precipitation has changed over time, for example, due to land

use change. The analysis also assumes a linear VOD response, which is an approximation to observed non-linear water-vegetation responses (Short Gianotti et al., 2019).

2.3. Application of Cross-Spectral Analysis to Observations

For each 0.25° pixel and each season, we compute the coherency and phase difference spectra if the pixel has VOD observations for at least 30% of days (after masking inundation). Coherency is estimated at approximately 150 frequencies spanning the 25–60-day band. When determining significance, we perform a robustness test by comparing the coherency spectra of nearby pixels, since we expect ISOs and the corresponding vegetation responses to occur at scales much larger than 0.25°. The "neighbors" of a pixel are defined as eight pixels in a square around it, such that all neighbors are separated by at least 0.75° (Figure S3 in Supporting Information S1). This separation avoids the comparison of VOD data that are derived from microwave measurements with overlapping footprints. Accounting for the width of the intraseasonal band, a pixel has a 95% significant coherent relationship for a period of x days if the pixel itself and at least three of its neighbors have coherency greater than the significance level (0.78) at some frequency within the resolution bandwidth around $\frac{1}{x}$ cycles per day. The intraseasonal coherency and phase difference are computed as averages across all periods in the intraseasonal band showing significant coherency. The 95% confidence interval for the phase difference is then derived from the average coherency. If phase differences exist near antiphase, the phase angles are shifted from $[-180°, 180°]$ to $[0°, 360°]$ before averaging, to avoid averaging two antiphase angles to appear in phase. As an additional step, two intraseasonal sub-bands corresponding to periods of 25–40 and 40–60 days were analyzed to ascertain possible differences between phase relationships.

3. Results

The sign of the phase difference between intraseasonal precipitation and VOD variations is shown in Figure 2 for all pixels with a coherent intraseasonal relationship at 95% significance. For small phase differences, the 95% confidence interval may overlap zero (yellow pixels), meaning that the sign of the phase difference cannot be determined from currently available observations. As expected, more phase differences are positive than negative, that is, VOD lags precipitation in more locations than it leads. Wet intraseasonal events increase soil moisture, enabling increased water uptake by vegetation and hence increased VOD. Approximately half of the roughly 194,000 pixels with a coherent precipitation-VOD relationship have a positive phase difference with 95% confidence. Many regions exhibit coherence in both bands, though for example, East Africa in MAM shows a coherent response only for 40–60-day variability. Examples of observed precipitation and VOD time series, with their estimated phase differences, are included in Figure S4 in Supporting Information S1.

Large areas with positive phase differences are found in arid or semi-arid regions (Figure 2), consistent with enhanced vegetation sensitivity in water-limited environments. The regions where we identify positive phase differences broadly correspond to locations where water availability is an important driver of vegetation productivity on climate timescales (Li et al., 2021; Papagiannopoulou et al., 2017; Seddon et al., 2016; Walther et al., 2019). In addition, most of these areas have a relatively high percentage of precipitation variance in the intraseasonal band (Figure S5 in Supporting Information S1, following Moron & Robertson, 2020). These regions are therefore the most likely to exhibit vegetation-induced evapotranspiration anomalies that provide a source of S2S predictability.

Changes in VOD mostly occur less than a week after precipitation (Figure 3, dashed lines). Of the pixels with a positive mean phase difference estimate in the 40–60-day band, 58% of these are within 7 days, increasing to 79% for the 25–40-day band. These responses are considerably shorter than the 1–3-month rainfall-vegetation lags computed in climatic studies using monthly data (e.g., Wu et al., 2015)—partly because the use of daily VOD data enables the resolution of sub-monthly responses. The responses to intraseasonal variability are longer than the time estimated for peak VOD to occur following short-term SSM anomalies, which is often only 1–2 days (Feldman, Short Gianotti et al., 2021; He et al., 2021). For longer wet spells, increases in biomass are more likely to occur, which are slower than the plant rehydration that dominates 1–2-day VOD responses (Feldman, Short Gianotti et al., 2021).

Despite applying our surface water mask, inundation still impacts VOD in regions such as India and Madagascar (in MAM). Such pixels exhibit decreased VOD due to inundation shortly after rainfall, resulting in large negative

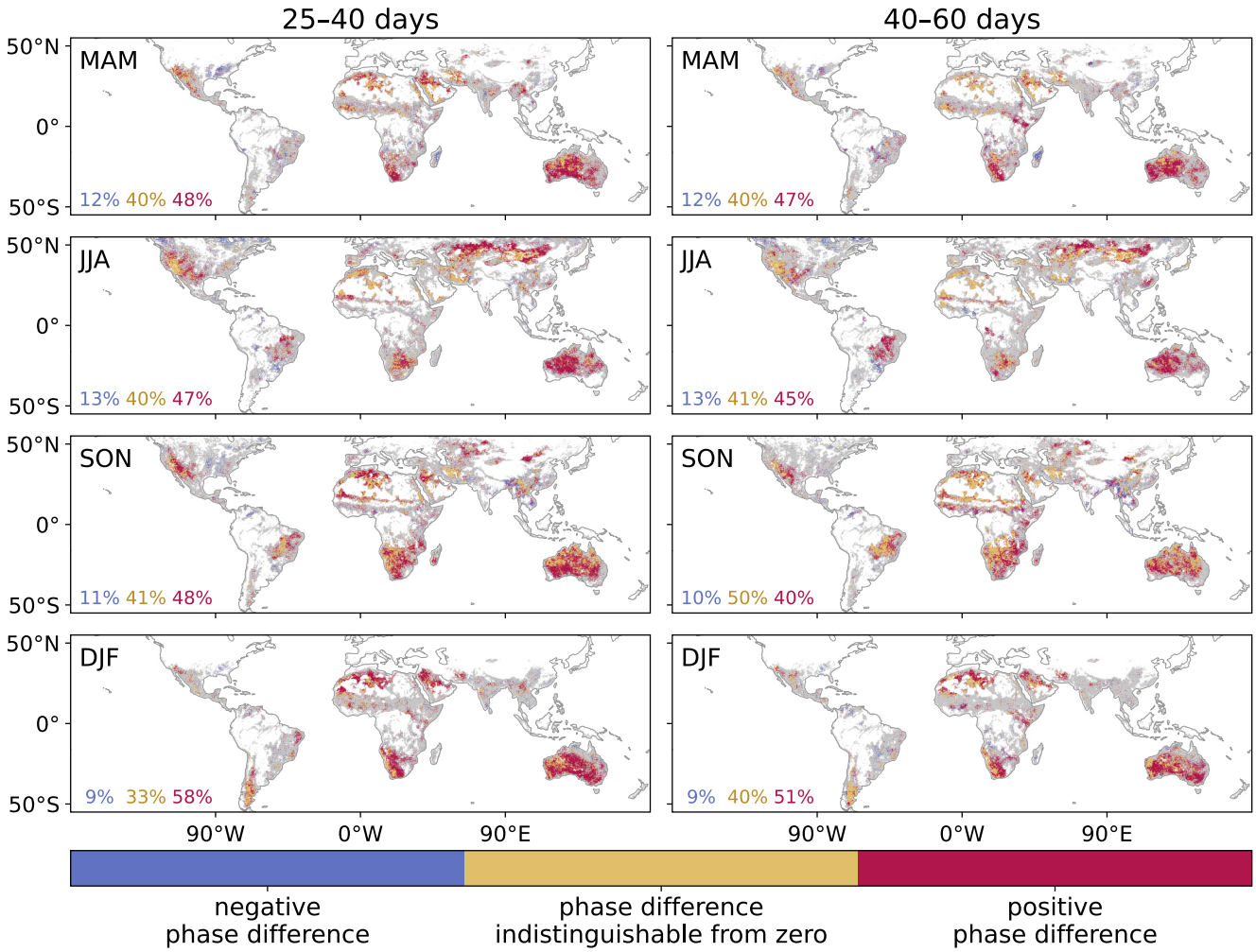

Figure 2. Sign of phase difference between intraseasonal precipitation and Vegetation Optical Depth (VOD) variability. Positive phase difference means VOD lags precipitation. Column titles show the periods of variability. White pixels denote too few observations for analysis whilst gray pixels denote that no 95% significant coherent relationship was found.

phase differences (Figure S4c in Supporting Information S1). Our mask does eliminate most of these negative phase differences: without masking VOD, 46% of 40–60-day phase differences are negative with 95% confidence, versus 11% after masking. Negative phase differences can also occur due to vegetation changes genuinely preceding precipitation changes, for example, in monsoonal northern Australia in DJF, where Green et al. (2017) argued that vegetation has a strong intraseasonal influence on precipitation. Also, in locations where vegetation is limited more by temperature or radiation than moisture, negative phase differences could result from dry spells favoring growth under warmer, less cloudy conditions.

To investigate whether the vegetation type influences the surface response to intraseasonal precipitation variability, Figure 3 shows the distributions of phase difference by land cover, aggregated over all seasons. The distributions are wider for 40–60-day variability than 25–40-day variability, with peaks at longer phase differences. The distributions for all land covers peak below 10 days. Sparsely vegetated areas, typically found in arid regions, typically have faster vegetation responses than other land covers, consistent with other studies (De Keersmaecker et al., 2015; Vicente-Serrano et al., 2013). In an arid climate, rapid vegetation green-up can occur in response to a wet spell. Indeed, Feldman et al. (2018) found the strongest vegetation water uptake following soil moisture pulses in regions with low rainfall.

Fewer pixels with a coherent precipitation-VOD relationship are found in forest and cropland (Figure S6 in Supporting Information S1). This is partly due to lack of data; these classes are frequently masked as inundated.

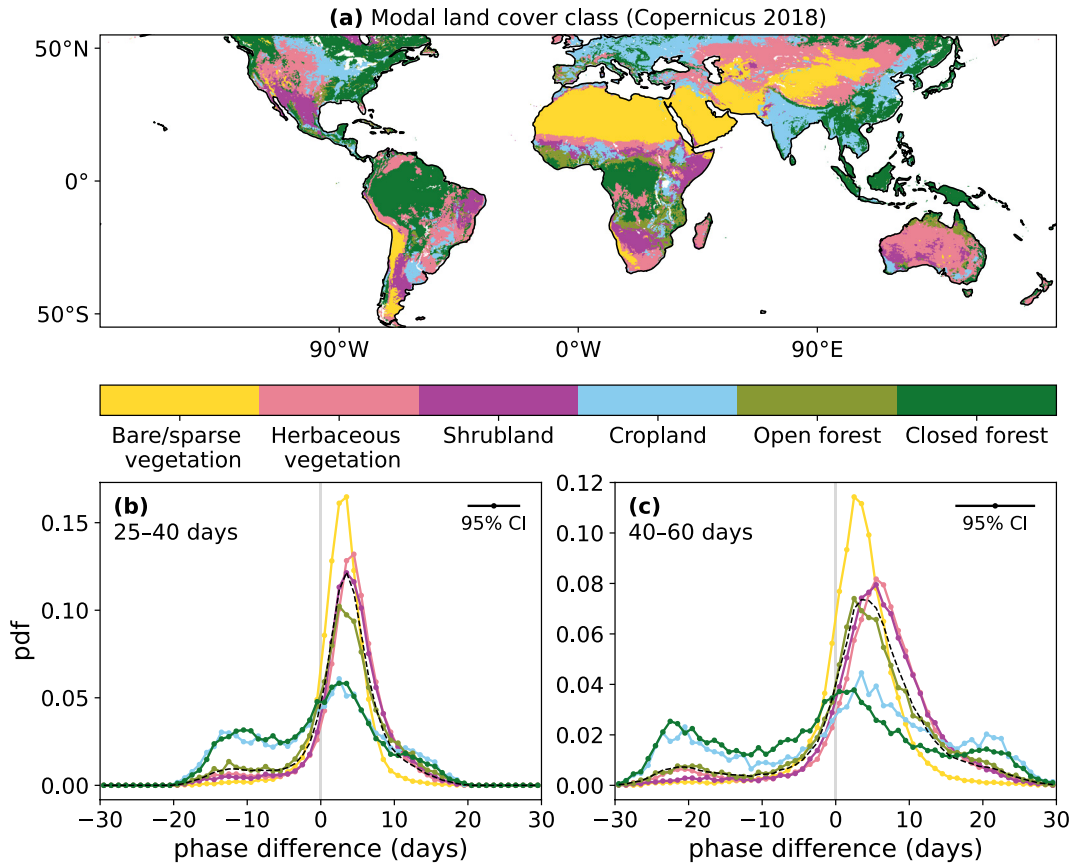

Figure 3. (a) 2018 Copernicus Global Land Service Land Cover map (Buchhorn et al., 2020), aggregated to 0.25°. (b, c) Probability distributions of phase difference between precipitation and Vegetation Optical Depth (all seasons), by land cover type, for (b) 25–40-day and (c) 40–60-day variability. Black dashed lines show the probability distribution for all land covers combined. Error bars show the median width of the 95% confidence interval over all pixels. The color bar applies to all panels.

For cropland this is potentially linked to irrigation. In forests, the inundation mask may over-mask due to the lack of SSM observations. Even with sufficient data we expect weaker precipitation impact on VOD for these land covers; forests tend to exhibit stronger radiation and temperature controls (e.g., Papagiannopoulou et al., 2017), whilst cropland will be affected by irrigation and harvesting. It is also more difficult to identify coherent relationships in forests because variations in the nearly-saturated VOD signal are small, heterogeneous canopy structures introduce errors into VOD retrievals (Konings et al., 2021), and VOD retrievals are more sensitive to noise for dense vegetation (Feldman, Chaparro, & Entekhabi, 2021).

Whilst cross-spectral analysis investigates the correlation and relative timing of precipitation and VOD variability, it does not provide information on the persistence of VOD anomalies following anomalous precipitation. For example, in the weeks after a wet event, VOD may quickly return to its prior state, or may maintain high values, particularly if the rain stimulated an increase in biomass. To investigate this, we construct composites around intraseasonal wet events. Applying a 25-day low-pass Lanczos filter to the day-of-year precipitation anomaly at each pixel, these events are defined as local maxima lying above one standard deviation from the mean of the filtered time series. We then composite standardized anomalies of precipitation, VOD and SSM from their daily climatology on the wet events. We similarly composite 16-day MODIS NDVI anomalies, using a monthly climatology. All data have any long-term linear trends removed prior to processing.

Figure 4 shows the composites of standardized anomalies for ±60 days around the precipitation event. Note that these composites focus only on strong wet spells, whereas the cross-spectral method analyzed the entire time series. Sparse vegetation, shrubland and herbaceous vegetation all show quick VOD responses to the precipitation, consistent with Figure 3. The SSM composites exhibit a much larger peak standardized anomaly than

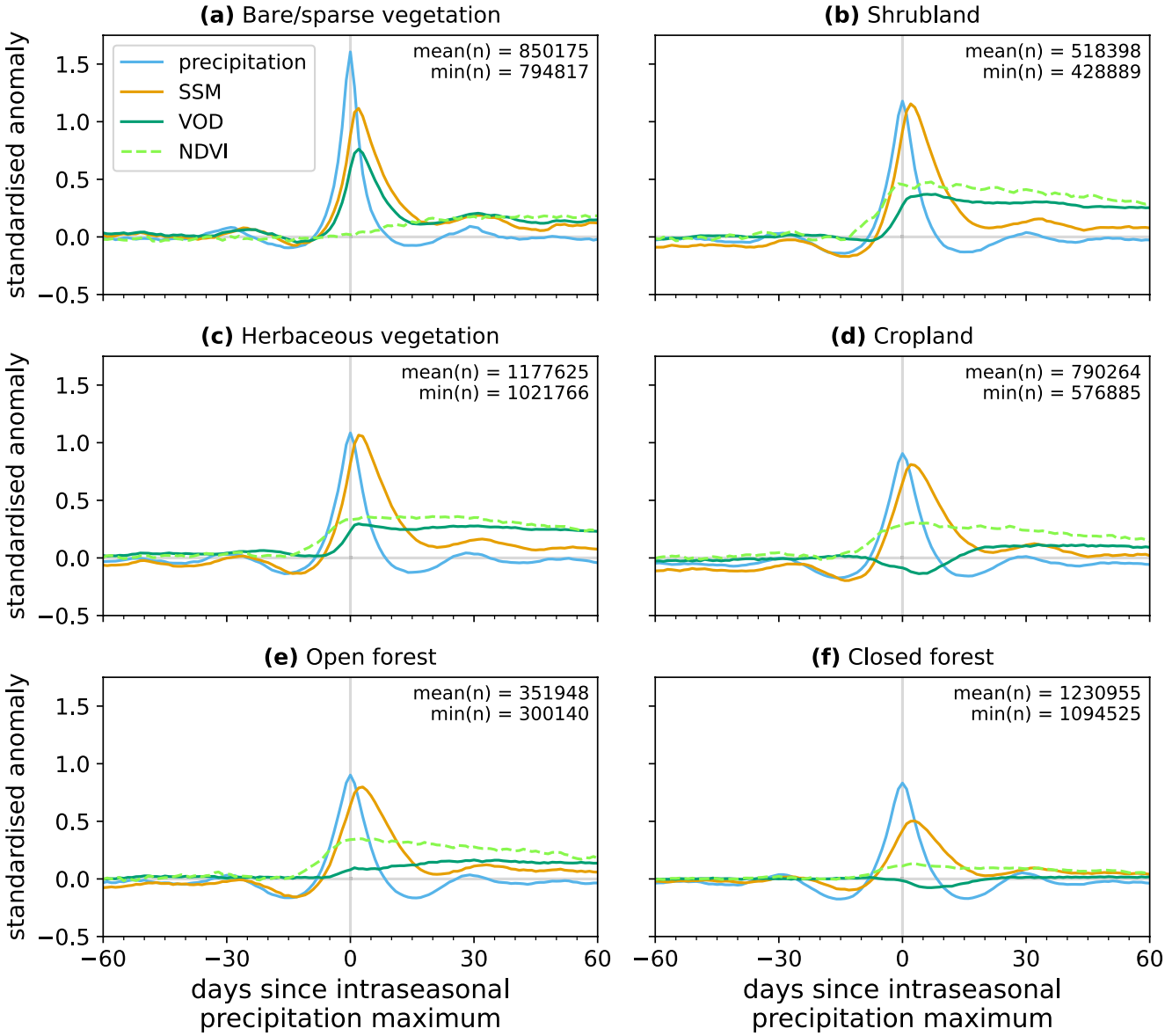

Figure 4. Standardized anomaly composites of precipitation, surface soil moisture, Vegetation Optical Depth, and Normalized Difference Vegetation Index (NDVI) around intraseasonal wet events, for all pixels from 55°S to 55°N. For any given number of days since the event, *n* is the number of observations that were averaged to create the composite at that time (*n* does not apply to NDVI composites).

VOD, but whereas the SSM anomaly declines over the following 10 days, the VOD anomaly in shrubland and herbaceous vegetation persists out to +60 days. A strong post-event signal is also evident in NDVI, indicating a persistent increase in biomass. Two months after the event, standardized anomalies of both VOD and NDVI are approximately twice that of SSM for these two classes. We also expect root zone soil moisture anomalies to persist longer than SSM, though we cannot observe this directly.

Sparse vegetation shows the largest standardized VOD anomaly in the days after rainfall, but this anomaly is short-lived. The similarity of the VOD and SSM composites is likely a consequence of the strong soil moisture control on vegetation in arid climates. However, we also acknowledge the potential for misattribution of the microwave signal between water in the soil and vegetation. A strong, short-lived NDVI response is not evident, but this could be due to the poorer temporal resolution. In both cropland and closed forest, VOD decreases during wet events, again suggesting inundation effects. Closed forest shows no evidence of a VOD increase, indicating a lack of water control. The VOD response of open forest can be understood as a combination of the herbaceous

vegetation and closed forest responses. Overall, this analysis highlights that the vegetation response to intraseasonal wet events depends on land cover type, with large persistent responses in herbaceous vegetation and shrubland. This suggests that vegetation responses could enhance S2S forecasts at longer lead times in these land covers, by providing a source of predictability (via transpiration) well beyond the intraseasonal event.

4. Discussion and Conclusions

Satellite-based measurements were used to identify coherent relationships between intraseasonal variability in precipitation and VOD. Across arid and semi-arid regions, VOD tends to increase in response to wet spells. For all land covers, the distribution of phase difference peaks at less than 10 days. Bare/sparsely vegetated areas respond fastest, consistent with dominant moisture control on vegetation processes. In a minority of pixels, predominantly covered by cropland and forest, precipitation variations significantly lag VOD. In forests, this may indicate a dominant temperature or insolation control, which tend to be in antiphase with precipitation. Croplands may be impacted by irrigation and harvesting. In many cases, it appears to be an artefact of transient inundation, which poses a significant challenge for the interpretation of VOD signals. Our methodology to limit the impact of surface water fraction changes results in large areas of the domain being masked, including India during the monsoon season.

Although VOD fluctuations predominantly lag precipitation, this does not mean that vegetation anomalies cannot influence subsequent precipitation. Our cross-spectral analysis treats the precipitation-vegetation system as linear and estimates a single value for the phase difference. The stronger vegetation response to precipitation is expected to dominate any weaker impacts in the opposing direction. Moreover, the impact of intraseasonal surface variability on precipitation may be non-local (Chug & Dominguez, 2019; Talib et al., 2021, 2022). Water controls on transpiration (rather than direct evaporation) provide the dominant pathway for atmospheric feedbacks on these timescales. Daily VOD observations are valuable because transpiration cannot be directly observed by satellites, but it is strongly affected by vegetation biomass and water stress, which are both represented in VOD. Overall, our results provide unique evidence of coherent intraseasonal relationships between precipitation and transpiration, their global distribution, and associated timescales.

Characterizing vegetation responses to intraseasonal precipitation variability is a prerequisite to understanding how vegetation-atmosphere feedbacks can support S2S predictability. ISOs typically impact precipitation on scales of several hundred to several thousand kilometers (Krishnamurthy & Shukla, 2008; Zhang et al., 2020). In regions highlighted in Figure 2, we expect these ISOs to induce coherent transpiration responses over similar scales. Perturbations in transpiration can affect surface heating of the lower atmosphere, influencing regional pressure gradients, low-level jets and moisture convergence. These changes, along with direct atmospheric moistening, can affect subsequent rainfall (Chug & Dominguez, 2019; Taylor, 2008; S. Zhou et al., 2021). To further support S2S forecast model development, future research should quantify the transpiration response to intraseasonal VOD perturbations and understand the atmospheric response to transpiration changes.

Given that realistic initialization of land surface conditions improves atmospheric predictability over S2S timescales (Koster et al., 2010), correctly representing the vegetation response to ISOs should further enhance predictability from vegetation-atmosphere feedbacks in the regions where the responses occur. For example, the MJO impacts precipitation across herbaceous regions of Australia (Wheeler et al., 2009). Current S2S forecast models demonstrate skill in predicting the MJO out to 3 weeks (Vitart, 2017). As we observe a vegetation response to intraseasonal rainfall variability with a lag of approximately 1 week in this area (Figures 2 and 3), we predict that a model that correctly represents the MJO-induced rainfall variability could gain additional skill by modeling the subsequent vegetation response. The persistence of the vegetation response (Figure 4c) also provides potential for a source of predictability beyond the 3-week lead time. However, the land surface response to intraseasonal variability in current S2S forecasts will be highly model-dependent, given the large spread of surface energy balance dynamics found in climate models on intraseasonal timescales (Gallego-Elvira et al., 2019). This implies a loss of skill in the forecast range identified by Dirmeyer et al. (2015), where land surface processes provide a bridge between sub-weekly predictability from the atmosphere and monthly predictability from oceanic conditions. Accurately representing intraseasonal vegetation variability offers potential to exploit this predictability.

Data Availability Statement

All datasets used for this work are freely available for download. IMERG precipitation: https://doi.org/10.5067/GPM/IMERGDF/DAY/06 (Huffman et al., 2019). VODCA: https://doi.org/10.5281/zenodo.2575599 (Moesinger et al., 2019). ESA CCI soil moisture: https://www.esa-soilmoisture-cci.org combined product v06.1 (accessed 23 July 2021). SWAMPS surface water fraction: https://asf.alaska.edu/data-sets/derived-data-sets/wetlands-measures/wetlands-measures-product-downloads/ global daily product v3.2 (accessed 23 June 2021). Copernicus Global Land Service land cover: https://doi.org/10.5281/zenodo.3518038 discrete classification map (Buchhorn et al., 2020). MODIS NDVI composites: Terra https://doi.org/10.5067/MODIS/MOD13C1.006 (Didan, 2015a), Aqua https://doi.org/10.5067/MODIS/MYD13C1.006 (Didan, 2015b). The code used to generate the results of the paper is available at https://doi.org/10.5281/zenodo.6783138. The code used for the cross-spectral analysis, csagan1.1f, is freely available for to anyone to use from the Met Office Science Repository Service at https://code.metoffice.gov.uk/trac/lmed/browser%23main/trunk/benchmarking (last access: 29 June 2022). Access requires registration for an account and this will be supported by a member of the JULES group. Requests for new accounts can be made by emailing Jules-Support@metoffice.gov.uk with details of the user's name, email address, institution and purpose for requiring access.

Acknowledgments
The work of BLH and CMT was supported by the NERC National Centre for Earth Observation (NCEO) under the Diagnosing Energy and Water Exchanges in the Earth System (DEWEES) project, Grant No. NE/R016518/1. JT was supported by UK Research and Innovation (UKRI) as part of the Global Challenges Research Fund, African Science for Weather Information and Forecasting Techniques (SWIFT) programme, Grant No. NE/P021077/1. We would like to thank Garry Hayman and Tristan Quaife for helpful discussions about the work, and Andrew Feldman and one anonymous reviewer for their valuable feedback.

References

Attema, E. P., & Ulaby, F. T. (1978). Vegetation modeled as a water cloud. *Radio Science*, *13*(2), 357–364. https://doi.org/10.1029/RS013I002P00357

Bousquet, E., Mialon, A., Rodriguez-Fernandez, N., Prigent, C., Wagner, F. H., & Kerr, Y. H. (2021). Influence of surface water variations on VOD and biomass estimates from passive microwave sensors. *Remote Sensing of Environment*, *257*, 112345. https://doi.org/10.1016/j.rse.2021.112345

Brunet, G., Shapiro, M., Hoskins, B., Moncrieff, M., Dole, R., Kiladis, G. N., et al. (2010). Collaboration of the weather and climate communities to advance subseasonal-to-seasonal prediction. *Bulletin of the American Meteorological Society*, *91*(10), 1397–1406. https://doi.org/10.1175/2010BAMS3013.1

Buchhorn, M., Smets, B., Bertels, L., Roo, B. D., Lesiv, M., Tsendbazar, N.-E., et al. (2020). Copernicus Global Land Service: Land Cover 100 m: Collection 3: Epoch 2018: Globe (v3.0.1) [Dataset]. Zenodo. https://doi.org/10.5281/ZENODO.3518038

Chug, D., & Dominguez, F. (2019). Isolating the observed influence of vegetation variability on the climate of La Plata River Basin. *Journal of Climate*, *32*(14), 4473–4490. https://doi.org/10.1175/JCLI-D-18-0677.1

Cissé, S., Eymard, L., Ottlé, C., Ndione, J. A., Gaye, A. T., & Pinsard, F. (2016). Rainfall intra-seasonal variability and vegetation growth in the Ferlo Basin (Senegal). *Remote Sensing*, *8*(1), 66. https://doi.org/10.3390/RS8010066

De Keersmaecker, W., Lhermitte, S., Tits, L., Honnay, O., Somers, B., & Coppin, P. (2015). A model quantifying global vegetation resistance and resilience to short-term climate anomalies and their relationship with vegetation cover. *Global Ecology and Biogeography*, *24*(5), 539–548. https://doi.org/10.1111/GEB.12279

Didan, K. (2015a). MOD13C1 MODIS/Terra Vegetation Indices 16-Day L3 Global 0.05Deg CMG V006 [Dataset]. NASA EOSDIS Land Processes DAAC. https://doi.org/10.5067/MODIS/MOD13C1.006

Didan, K. (2015b). MYD13C1 MODIS/Aqua Vegetation Indices 16-Day L3 Global 0.05Deg CMG V006 [Dataset]. NASA EOSDIS Land Processes DAAC. https://doi.org/10.5067/MODIS/MYD13C1.006

Ding, R., Li, J., & Seo, K.-H. (2011). Estimate of the predictability of boreal summer and winter intraseasonal oscillations from observations. *Monthly Weather Review*, *139*(8), 2421–2438. https://doi.org/10.1175/2011MWR3571.1

Dirmeyer, P. A., Halder, S., & Bombardi, R. (2018). On the harvest of predictability from land states in a global forecast model. *Journal of Geophysical Research: Atmospheres*, *123*(23), 13111–13127. https://doi.org/10.1029/2018JD029103

Dirmeyer, P. A., Peters-Lidard, C., & Balsamo, G. (2015). Land-atmosphere interactions and the water cycle. In G. Brunet, S. Jones, & P. M. Ruti (Eds.), *Seamless prediction of the earth system: From minutes to months* (pp. 145–154). World Meteorological Organization. Retrieved from https://public.wmo.int/en/resources/library/seamless-prediction-of-earth-system-from-minutes-months

Dorigo, W., Wagner, W., Albergel, C., Albrecht, F., Balsamo, G., Brocca, L., et al. (2017). ESA CCI Soil Moisture for improved Earth system understanding: State-of-the art and future directions. *Remote Sensing of Environment*, *203*, 185–215. https://doi.org/10.1016/J.RSE.2017.07.001

Feldman, A. F., Chaparro, D., & Entekhabi, D. (2021). Error propagation in microwave soil moisture and vegetation optical depth retrievals. *IEEE Journal of Selected Topics in Applied Earth Observations and Remote Sensing*, *14*, 11311–11323. https://doi.org/10.1109/JSTARS.2021.3124857

Feldman, A. F., Short Gianotti, D. J., Konings, A. G., Gentine, P., & Entekhabi, D. (2021). Patterns of plant rehydration and growth following pulses of soil moisture availability. *Biogeosciences*, *18*(3), 831–847. https://doi.org/10.5194/BG-18-831-2021

Feldman, A. F., Short Gianotti, D. J., Konings, A. G., McColl, K. A., Akbar, R., Salvucci, G. D., & Entekhabi, D. (2018). Moisture pulse-reserve in the soil-plant continuum observed across biomes. *Nature Plants*, *4*(12), 1026–1033. https://doi.org/10.1038/s41477-018-0304-9

Ferranti, L., Slingo, J. M., Palmer, T. N., & Hoskins, B. J. (1999). The effect of land-surface feedbacks on the monsoon circulation. *Quarterly Journal of the Royal Meteorological Society*, *125*(557), 1527–1550. https://doi.org/10.1002/qj.49712555704

Gallego-Elvira, B., Taylor, C. M., Harris, P. P., & Ghent, D. (2019). Evaluation of regional-scale soil moisture-surface flux dynamics in Earth System Models based on satellite observations of land surface temperature. *Geophysical Research Letters*, *46*(10), 5480–5488. https://doi.org/10.1029/2019GL082962

Green, J. K., Konings, A. G., Alemohammad, S. H., Berry, J., Entekhabi, D., Kolassa, J., et al. (2017). Regionally strong feedbacks between the atmosphere and terrestrial biosphere. *Nature Geoscience*, *10*(6), 410–414. https://doi.org/10.1038/ngeo2957

Gruber, A., Scanlon, T., Van Der Schalie, R., Wagner, W., & Dorigo, W. (2019). Evolution of the ESA CCI Soil Moisture climate data records and their underlying merging methodology. *Earth System Science Data*, *11*(2), 717–739. https://doi.org/10.5194/ESSD-11-717-2019

Guo, Z., Dirmeyer, P. A., & Delsole, T. (2011). Land surface impacts on subseasonal and seasonal predictability. *Geophysical Research Letters*, *38*(24). https://doi.org/10.1029/2011GL049945

Guo, Z., Dirmeyer, P. A., Delsole, T., & Koster, R. D. (2012). Rebound in atmospheric predictability and the role of the land surface. *Journal of Climate*, *25*(13), 4744–4749. https://doi.org/10.1175/JCLI-D-11-00651.1

He, Q., Lu, H., Yang, K., Zhen, L., Yue, S., Li, Y., & Entekhabi, D. (2021). Global patterns of vegetation response to short-term surface water availability. *IEEE Journal of Selected Topics in Applied Earth Observations and Remote Sensing*, *14*, 8273–8286. https://doi.org/10.1109/JSTARS.2021.3103854

Huffman, G., Stocker, E., Bolvin, D., Nelkin, E., & Tan, J. (2019). *GPM IMERG Final Precipitation L3 1 day 0.1 degree × 0.1 degree v06, Edited by Andrey Savtchenko*. Goddard Earth Sciences Data and Information Services Center (GES DISC). https://doi.org/10.5067/GPM/IMERGDF/DAY/06

Jackson, T. J., & Schmugge, T. J. (1991). Vegetation effects on the microwave emission of soils. *Remote Sensing of Environment*, *36*(3), 203–212. https://doi.org/10.1016/0034-4257(91)90057-D

Jensen, K., & Mcdonald, K. (2019). Surface water microwave product series Version 3: A near-real time and 25-year historical global inundated area fraction time series from active and passive microwave remote sensing. *IEEE Geoscience and Remote Sensing Letters*, *16*(9), 1402–1406. https://doi.org/10.1109/lgrs.2019.2898779

Jones, M. O., Jones, L. A., Kimball, J. S., & McDonald, K. C. (2011). Satellite passive microwave remote sensing for monitoring global land surface phenology. *Remote Sensing of Environment*, *115*(4), 1102–1114. https://doi.org/10.1016/J.RSE.2010.12.015

Justice, C. O., Dugdale, F., Townshend, J. R., Narracott, A. S., & Kumar, M. (1991). Synergism between NOAA-AVHRR and Meteosat data for studying vegetation development in semi-arid West Africa. *International Journal of Remote Sensing*, *12*(6), 1349–1368. https://doi.org/10.1080/01431169108929730

Konings, A. G., Saatchi, S. S., Frankenberg, C., Keller, M., Leshyk, V., Anderegg, W. R., et al. (2021). Detecting forest response to droughts with global observations of vegetation water content. *Global Change Biology*, *27*(23), 6005–6024. https://doi.org/10.1111/GCB.15872

Koster, R. D., Mahanama, S. P., Yamada, T. J., Balsamo, G., Berg, A. A., Boisserie, M., et al. (2010). Contribution of land surface initialization to subseasonal forecast skill: First results from a multi-model experiment. *Geophysical Research Letters*, *37*(2). https://doi.org/10.1029/2009GL041677

Koster, R. D., Schubert, S. D., Deangelis, A. M., Molod, A. M., & Mahanama, S. P. (2020). Using a simple water balance framework to quantify the impact of soil moisture initialization on subseasonal evapotranspiration and air temperature forecasts. *Journal of Hydrometeorology*, *21*(8), 1705–1722. https://doi.org/10.1175/JHM-D-20-0007.1

Krishnamurthy, V., & Shukla, J. (2008). Seasonal persistence and propagation of intraseasonal patterns over the Indian monsoon region. *Climate Dynamics*, *30*(4), 353–369. https://doi.org/10.1007/S00382-007-0300-7/FIGURES/14

Lavender, S. L., Taylor, C. M., & Matthews, A. J. (2010). Coupled land-atmosphere intraseasonal variability of the West African monsoon in a GCM. *Journal of Climate*, *23*(21), 5557–5571. https://doi.org/10.1175/2010JCLI3419.1

Li, W., Migliavacca, M., Forkel, M., Walther, S., Reichstein, M., & Orth, R. (2021). Revisiting global vegetation controls using multi-layer soil moisture. *Geophysical Research Letters*, *48*(11), e2021GL092856. https://doi.org/10.1029/2021GL092856

Madden, R. A., & Julian, P. R. (1994). Observations of the 40–50-day tropical oscillation—A review. *Monthly Weather Review*, *122*(5), 814–837. https://doi.org/10.1175/1520-0493(1994)122%3C0814:OOTDTO%3E2.0.CO;2

McColl, K. A., Wang, W., Peng, B., Akbar, R., Short Gianotti, D. J., Lu, H., et al. (2017). Global characterization of surface soil moisture drydowns. *Geophysical Research Letters*, *44*(8), 3682–3690. https://doi.org/10.1002/2017GL072819

Meesters, A. G., De Jeu, R. A., & Owe, M. (2005). Analytical derivation of the vegetation optical depth from the microwave polarization difference index. *IEEE Geoscience and Remote Sensing Letters*, *2*(2), 121–123. https://doi.org/10.1109/LGRS.2005.843983

Mo, T., Choudhury, B. J., Schmugge, T. J., Wang, J. R., & Jackson, T. J. (1982). A model for microwave emission from vegetation-covered fields. *Journal of Geophysical Research*, *87*(C13), 11229–11237. https://doi.org/10.1029/JC087IC13P11229

Moesinger, L., Dorigo, W., de Jeu, R., van der Schalie, R., Scanlon, T., Teubner, I., & Forkel, M. (2020). The Global Long-term Microwave Vegetation Optical Depth Climate Archive (VODCA). *Earth System Science Data*, *12*(1), 177–196. https://doi.org/10.5194/essd-12-177-2020

Moesinger, L., Dorigo, W., Jeu, R. D., der Schalie, R. V., Scanlon, T., Teubner, I., & Forkel, M. (2019). The Global Long-term Microwave Vegetation Optical Depth Climate Archive VODCA (1.0) [Dataset]. Zenodo. https://doi.org/10.5281/ZENODO.2575599

Moron, V., & Robertson, A. W. (2020). Tropical rainfall subseasonal-to-seasonal predictability types. *npj Climate and Atmospheric Science*, *3*(1), 4. https://doi.org/10.1038/s41612-020-0107-3

Nicholson, S. E., Davenport, M. L., & Malo, A. R. (1990). A comparison of the vegetation response to rainfall in the Sahel and East Africa, using normalized difference vegetation index from NOAA AVHRR. *Climatic Change*, *17*(2–3), 209–241. https://doi.org/10.1007/BF00138369

Papagiannopoulou, C., Miralles, D. G., Dorigo, W. A., Verhoest, N. E. C., Depoorter, M., & Waegeman, W. (2017). Vegetation anomalies caused by antecedent precipitation in most of the world. *Environmental Research Letters*, *12*(7), 074016. https://doi.org/10.1088/1748-9326/AA7145

Peng, J., Loew, A., & Crueger, T. (2017). The relationship between the Madden-Julian oscillation and the land surface soil moisture. *Remote Sensing of Environment*, *203*, 226–239. https://doi.org/10.1016/j.rse.2017.07.004

Rodríguez-Fernández, N. J., Mialon, A., Mermoz, S., Bouvet, A., Richaume, P., Al Bitar, A., et al. (2018). An evaluation of SMOS L-band vegetation optical depth (L-VOD) data sets: High sensitivity of L-VOD to above-ground biomass in Africa. *Biogeosciences*, *15*(14), 4627–4645. https://doi.org/10.5194/BG-15-4627-2018

Saha, S. K., Halder, S., Suryachandra Rao, A., & Goswami, B. N. (2012). Modulation of ISOs by land-atmosphere feedback and contribution to the interannual variability of Indian summer monsoon. *Journal of Geophysical Research*, *117*(D13). https://doi.org/10.1029/2011JD017291

Seddon, A. W. R., Macias-Fauria, M., Long, P. R., Benz, D., & Willis, K. J. (2016). Sensitivity of global terrestrial ecosystems to climate variability. *Nature*, *531*(7593), 229–232. https://doi.org/10.1038/nature16986

Short Gianotti, D. J., Rigden, A. J., Guido, D., Salvucci, G. D., & Entekhabi, D. (2019). Satellite and station observations demonstrate water availability's effect on continental-scale evaporative and photosynthetic land surface dynamics. *Water Resources Research*, *55*(1), 540–554. https://doi.org/10.1029/2018WR023726

Spennemann, P. C., & Saulo, A. C. (2015). An estimation of the land-atmosphere coupling strength in South America using the Global Land Data Assimilation System. *International Journal of Climatology*, *35*(14), 4151–4166. https://doi.org/10.1002/JOC.4274

Talib, J., Taylor, C. M., Duan, A., & Turner, A. G. (2021). Intraseasonal soil moisture–atmosphere feedbacks on the Tibetan Plateau circulation. *Journal of Climate*, *34*(5), 1789–1807. https://doi.org/10.1175/JCLI-D-20-0377.1

Talib, J., Taylor, C. M., Klein, C., Harris, B. L., Anderson, S. R., & Semeena, V. S. (2022). The sensitivity of the West African monsoon circulation to intraseasonal soil moisture feedbacks. *Quarterly Journal of the Royal Meteorological Society*, *148*(745), 1709–1730. https://doi.org/10.1002/qj.4274

Taylor, C. M. (2008). Intraseasonal land–atmosphere coupling in the West African monsoon. *Journal of Climate*, *21*(24), 6636–6648. https://doi.org/10.1175/2008JCLI2475.1

Teubner, I. E., Forkel, M., Jung, M., Liu, Y. Y., Miralles, D. G., Parinussa, R., et al. (2018). Assessing the relationship between microwave vegetation optical depth and gross primary production. *International Journal of Applied Earth Observation and Geoinformation*, *65*, 79–91. https://doi.org/10.1016/J.JAG.2017.10.006

Tian, F., Brandt, M., Liu, Y. Y., Verger, A., Tagesson, T., Diouf, A. A., et al. (2016). Remote sensing of vegetation dynamics in drylands: Evaluating vegetation optical depth (VOD) using AVHRR NDVI and in situ green biomass data over West African Sahel. *Remote Sensing of Environment*, *177*, 265–276. https://doi.org/10.1016/J.RSE.2016.02.056

Tian, F., Wigneron, J. P., Ciais, P., Chave, J., Ogée, J., Peñuelas, J., et al. (2018). Coupling of ecosystem-scale plant water storage and leaf phenology observed by satellite. *Nature Ecology and Evolution*, *2*(9), 1428–1435. https://doi.org/10.1038/s41559-018-0630-3

Unnikrishnan, C. K., Rajeevan, M., & Vijaya Bhaskara Rao, S. (2017). A study on the role of land-atmosphere coupling on the south Asian monsoon climate variability using a regional climate model. *Theoretical and Applied Climatology*, *127*(3), 949–964. https://doi.org/10.1007/S00704-015-1680-Y

van Hoek, M., Jia, L., Zhou, J., Zheng, C., & Menenti, M. (2016). Early drought detection by spectral analysis of satellite time series of precipitation and normalized difference vegetation index (NDVI). *Remote Sensing*, *8*(5), 422. https://doi.org/10.3390/rs8050422

van der Schalie, R., de Jeu, R. A., Kerr, Y. H., Wigneron, J. P., Rodríguez-Fernández, N. J., Al-Yaari, A., et al. (2017). The merging of radiative transfer based surface soil moisture data from SMOS and AMSR-E. *Remote Sensing of Environment*, *189*, 180–193. https://doi.org/10.1016/J.RSE.2016.11.026

Vicente-Serrano, S. M., Gouveia, C., Camarero, J. J., Beguería, S., Trigo, R., López-Moreno, J. I., et al. (2013). Response of vegetation to drought time-scales across global land biomes. *Proceedings of the National Academy of Sciences*, *110*(1), 52–57. https://doi.org/10.1073/PNAS.1207068110

Vitart, F. (2017). Madden-Julian Oscillation prediction and teleconnections in the S2S database. *Quarterly Journal of the Royal Meteorological Society*, *143*(706), 2210–2220. https://doi.org/10.1002/QJ.3079

Vitart, F., Ardilouze, C., Bonet, A., Brookshaw, A., Chen, M., Codorean, C., et al. (2017). The subseasonal to seasonal (S2S) prediction project database. *Bulletin of the American Meteorological Society*, *98*(1), 163–173. https://doi.org/10.1175/BAMS-D-16-0017.1

Waliser, D. E., Lau, K. M., Stern, W., & Jones, C. (2003). Potential predictability of the Madden–Julian Oscillation. *Bulletin of the American Meteorological Society*, *84*(1), 33–50. https://doi.org/10.1175/BAMS-84-1-33

Walther, S., Duveiller, G., Jung, M., Guanter, L., Cescatti, A., & Camps-Valls, G. (2019). Satellite observations of the contrasting response of trees and grasses to variations in water availability. *Geophysical Research Letters*, *46*(3), 1429–1440. https://doi.org/10.1029/2018GL080535

Webster, P. J. (1983). Mechanisms of monsoon low-frequency variability: Surface hydrological effects. *Journal of the Atmospheric Sciences*, *40*(9), 2110–2124. https://doi.org/10.1175/1520-0469(1983)040

Weedon, G. P., Prudhomme, C., Crooks, S., Ellis, R. J., Folwell, S. S., & Best, M. J. (2015). Evaluating the performance of hydrological models via cross-spectral analysis: Case study of the Thames Basin, United Kingdom. *Journal of Hydrometeorology*, *16*(1), 214–231. https://doi.org/10.1175/JHM-D-14-0021.1

Wheeler, M. C., Hendon, H. H., Cleland, S., Meinke, H., & Donald, A. (2009). Impacts of the Madden–Julian Oscillation on Australian rainfall and circulation. *Journal of Climate*, *22*(6), 1482–1498. https://doi.org/10.1175/2008JCLI2595.1

Wild, B., Teubner, I., Moesinger, L., Zotta, R.-M., Forkel, M., van der Schalie, R., et al. (2022). VODCA2GPP—A new, global, long-term (1988–2020) gross primary production dataset from microwave remote sensing. *Earth System Science Data*, *14*(3), 1063–1085. https://doi.org/10.5194/essd-14-1063-2022

Wu, D., Zhao, X., Liang, S., Zhou, T., Huang, K., Tang, B., & Zhao, W. (2015). Time-lag effects of global vegetation responses to climate change. *Global Change Biology*, *21*(9), 3520–3531. https://doi.org/10.1111/gcb.12945

Yu, Y., & Notaro, M. (2020). Observed land surface feedbacks on the Australian monsoon system. *Climate Dynamics*, *54*(5), 3021–3040. https://doi.org/10.1007/S00382-020-05154-0

Zhang, C., Adames, F., Khouider, B., Wang, B., & Yang, D. (2020). Four theories of the Madden-Julian Oscillation. *Reviews of Geophysics*, *58*(3), e2019RG000685. https://doi.org/10.1029/2019RG000685

Zhou, J., Jia, L., Menenti, M., van Hoek, M., Lu, J., Zheng, C., et al. (2021). Characterizing vegetation response to rainfall at multiple temporal scales in the Sahel-Sudano-Guinean region using transfer function analysis. *Remote Sensing of Environment*, *252*, 112108. https://doi.org/10.1016/j.rse.2020.112108

Zhou, S., Williams, A. P., Lintner, B. R., Berg, A. M., Zhang, Y., Keenan, T. F., et al. (2021). Soil moisture–atmosphere feedbacks mitigate declining water availability in drylands. *Nature Climate Change*, *11*(1), 38–44. https://doi.org/10.1038/s41558-020-00945-z

Zhu, H., Chen, H., Zhou, Y., Dong, X., Hanchen, Z., Haishan, C., & Xuan, D. (2019). Evaluation of the subseasonal forecast skill of surface soil moisture in the S2S database. *Atmospheric and Oceanic Science Letters*, *12*(6), 467–474. https://doi.org/10.1080/16742834.2019.1663123